Lab on a Chip

Cite this: *Lab Chip*, 2012, **12**, 2600–2611

www.rsc.org/loc

FOCUS

Acoustofluidics 15: streaming with sound waves interacting with solid particles

S. S. Sadhal

DOI: 10.1039/c2lc40243b

In Part 15 of the tutorial series "*Acoustofluidics—exploiting ultrasonic standing waves forces and acoustic streaming in microfluidic systems for cell and particle manipulation*," we examine the interaction of acoustic fields with solid particles. The main focus here is the interaction of standing waves with spherical particles leading to streaming, together with some discussion on one non-spherical case. We begin with the classical problem of a particle at the velocity antinode of a standing wave, and then treat the problem of a sphere at the velocity node, followed by the intermediate situation of a particle between nodes. Finally, we discuss the effect of deviation from sphericity which brings about interesting fluid mechanics. The entire Focus article is devoted to the analysis of the nonlinear fluid mechanics by singular perturbation methods, and the study of the streaming phenomenon that ensues from the nonlinear interaction. With the intention of being instructive material, this tutorial cannot by any means be considered 'complete and comprehensive' owing to the complexity of the class of problems being covered herein.

Department of Aerospace and Mechanical Engineering, University of Southern California, Los Angeles, CA, 90089-1453, USA

S. S. Sadhal

Prof. Satwindar Singh Sadhal received his B.A.Sc. in Engineering Science (Nuclear Power) and M.A.Sc. (Mechanical Engineering) from the University of Toronto in 1975 and 1976, and his Ph.D in Engineering Science from Caltech in 1978. He joined the University of Pennsylvania in 1978, and in 1982 moved to the University of Southern California (USC) where he has been a faculty member since, and was promoted to full Professor in 1994. He was a visiting Fellow at Clare Hall College (Cambridge) during 1988–89, and is now a Life Fellow. His research encompasses work on fluid dynamics, and heat/mass transfer, biotransport phenomena, and nonlinear acoustics in which he has published over a hundred refereed journal papers and conference proceedings. He was elected to Fellow of the American Society of Mechanical Engineers (ASME) in 1996 and was the recipient of the ASME James H. Potter Gold Medal in Thermodynamics (2007). His current research includes fundamental work on ocular fluid dynamics and transport phenomena with application to retinal drug delivery.

1 Introduction

When particles interact with high-frequency sound waves, streaming phenomenon occurs. As mentioned in tutorials 2 and 13,[1,23] the presence of solid surfaces in an acoustic field brings about a time-independent mean flow which we refer to as streaming. This type of interaction is very common with acoustic levitation devices. Such systems are used for container-less processing, and applications include non-contact trapping of cells and particle-based assays in continuous flow microsystems. For example, an acoustic standing wave is generated in etched glass micro-channels by miniature ultrasonic

Foreword

In the fifteenth paper of 23 in the *Lab on a Chip* tutorial series of Acoustofluidics, Satwindar Sadhal investigates acoustic streaming as a result of sound waves interacting with solid particles. Theoretical modules include particles positioned at velocity nodes and velocity anti nodes, as well as being positioned between nodes. Examples of spherical particles and oblate particles are presented.

Andreas Lenshof – coordinator of the Acoustofluidics series

transducers, and particles or cells passing the transducer can be retained and levitated at the center of the channel without any contact with the channel walls.[2] The potential of ultrasonic standing wave fields to facilitate viral transduction rate has been demonstrated by Lee & Peng.[10] Under acoustic exposure, suspended cells move to the pressure nodal planes first and form cell clusters. Then, viruses circulated between nodal planes use the pre-formed cell clusters as the nucleating sites to attach on to. In the past, several macroscale applications of acoustic levitation have been demonstrated, including non-contact thermophysical property measurement of liquids.[12,13] The suspension of liquid drops will be addressed in tutorial 16.[24]

In the absence of solid boundaries, simple sound waves usually have an irrotational character. Interaction with solid boundaries generates vorticity whereby nonlinearities set in within a thin layer (called the Stokes layer or the shear-wave layer) at the boundary. As discussed in tutorials 2 and 13,[1,23] nonlinearities can lead to a steady flow component that we refer to as streaming. This steady streaming persists outside the Stokes layer with vorticity.

This physical phenomenon may be characterized by considering a body of typical dimension a that oscillates with frequency ω and velocity $U_0\cos(\omega t)$ in a viscous fluid. If the parameter $\varepsilon = U_0/\omega a \ll 1$, then, although the leading order solution in powers of ε is oscillatory, higher order terms include not only higher harmonics but steady contributions to the velocity. This can be explained mathematically by existence of the nonlinear terms which may have a steady non-zero component. For high frequency we apply the condition $\varepsilon \ll 1$, which implies that the amplitude of the oscillation is small compared with a.

The existence of such steady streaming was first pointed out by Rayleigh[14] in his work on Kundt's dust tube and was later studied in the boundary layer context by Schlichting[25] who considered flows with the additional constraint $|M|^2 = \omega a^2/\nu \gg 1$, where ν denotes the kinematic viscosity of the fluid. Here, the parameter $|M|$ is also known as the Womersley number with the notation α. For such a flow it is now well established that the first order fluctuation vorticity is confined to a Stokes layer region of thickness $O((\nu/\omega)^{1/2}) = O(a/|M|)$, beyond which steady velocities $O(\varepsilon U_0)$ persist. At leading order in ε, the bulk of the flow is irrotational with zero mean over time. To $O(\varepsilon)$, this region has a non-zero time-averaged velocity field. As mentioned earlier, this steady flow is referred to as streaming that propagates into the bulk. The analytical procedure that we follow consists of perturbation expansions in small ε and large $|M|$. Since ε appears in front of the highest derivative in the momentum equation (see *e.g.*, the review by Riley[22]), the expansion procedure needs to be singular in character. This requires inner and outer expansions with stretching of the inner variable. However, it should be noted that if we were interested only in the outer-region streaming, the procedure developed by Nyborg[11] could be employed. With this procedure, the leading-order nonlinear terms when time-averaged, appear effectively as a conservative force in the next order. This method has been applied by Lee & Wang[9] for outer streaming associated with flow between parallel plates, as well the sphere and the cylinder placed between velocity node and antinode. Further extension of Nyborg's procedure,[11] has been recently carried out by Rednikov & Sadhal,[18] with the inclusion of non-adiabatic effects. Nevertheless, in order to fully understand streaming within the Stokes layer, inner and outer perturbation analysis is necessary.

Microfluidic applications and the relevance of streaming in liquids has been discussed by Bruus[1] in tutorial 2, as well as in tutorials 13[23] and 14.[27] For micron-sized particles, the flow-visualization work of Hagsäter *et al.*[4] is of importance in contrasting the streaming-based Stokes drag with the radiation force. They observed that at 2.17 MHz on 1 μm polystyrene beads, the Stokes drag is higher than the radiation force, while on 5 μm beads, the latter is dominant. It should be noted here that the Stokes layer thickness for this frequency is close to 1 μm, *i.e.*, $(\nu/\omega)^{1/2} \sim 1$ μm, corresponding to $|M| \sim 1$ in the case of a 1 μm particle.

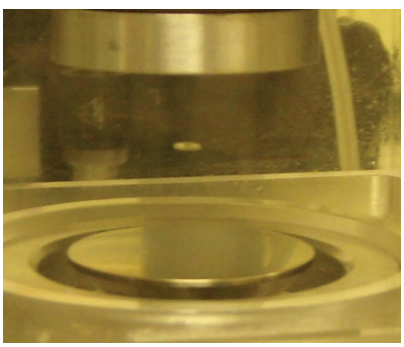

Fig. 1 Ultrasound levitation apparatus. The picture shows a levitated water-alcohol drop, approximately 3 mm across and 1 mm high. The bottom plate is an ultrasound transducer operating at 20 kHz, and the top is a slightly cupped reflector so that the system produces a standing wave.

1.1 Acoustic levitators

A typical desktop levitator is shown in Fig. 1. The main physical principle involved here is that the acoustic field provides the radiation pressure necessary to levitate a liquid drop in a gravitational field. The studies on the effects of radiation pressure on spheres and disks goes as far back as the 1930s. Some of the earliest theoretical studies were carried out by King.[6,7] With the application of this principle, ultrasound levitators have been in use for many years in ground-based experiments (as opposed to space-based). With the widespread application of levitation systems in the 1980s and 90s, there has been an interest in understanding the fluid-flow fundamentals associated with these systems. Some of the earlier work to characterize this flow include the developments of Trinh & Robey.[26] An example of their work on streaming flow visualization around a levitated drop is given in Fig. 2.

Among the items of interest is the information about the characteristics of the levitation process. For example, with

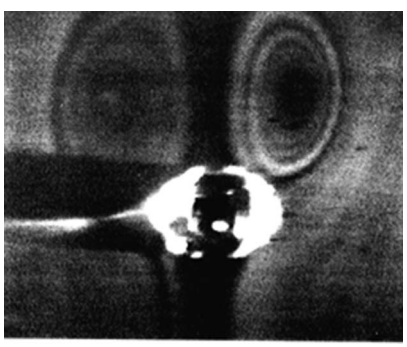

Fig. 2 Visualization of streaming around a levitated particle. The tested particle is a drop of water with diameter 1.8–1.85 mm. The acoustic frequency is 37 kHz, corresponding to $|M| \simeq 110$.[26]

acoustically-levitated particles there is a residual flow field including solid-body rotation for drops. For levitation under near zero-gravity conditions, the drop assumes an equilibrium position at the velocity antinode when the external medium is a gas (see Fig. 2 in tutorial 13[23] for node and antinode definitions). If the particle phase is a fluid with higher compressibility than the external phase (*e.g.*, a gas bubble in a liquid), the equilibrium position can occur at the velocity node. While the antinode solution has been available from Riley's[21] classical work, the node solution is relatively more recent.

For a levitated spherical particle positioned at the velocity antinode, Riley's solution[21] of a vibrating sphere in an otherwise quiescent fluid can be accommodated for $a/\lambda = a\omega/c \ll 1$, *i.e.*, when the particle size is small compared with the wavelength of the standing wave. In the next section, we discuss Riley's solution.[21] However, before we go to that development, we shall state the equations of motion for the class of problems discussed in this tutorial.

1.2 Equations of motion

The equations of continuity and momentum as relevant to acoustics are given in tutorial 2 and 13.[1,23] In particular, reference is made to eqn (1) and (3) in tutorial 13.[23] We apply the dimensionless scaling,

$$\begin{aligned} &\boldsymbol{u}=\frac{\boldsymbol{u}'}{U_0}, \quad \psi=\frac{\psi'}{U_0a^2}, \quad \varphi=\frac{\varphi'}{U_0a} \\ &\boldsymbol{x}=\frac{\boldsymbol{x}'}{a}, \quad t=\omega t', \quad p=\frac{p'}{\rho_0U_0\omega a} \\ &\rho=\frac{\rho'c^2}{\rho_0U_0\omega a}, \quad \nabla=a\nabla', \end{aligned} \tag{1}$$

for velocity, axisymmetric stream function, velocity potential, coordinate variables, time, pressure, density and the gradient operator, respectively. Here the typical system constants are U_0, a, ω, ρ_0 and p_0, representing velocity, length scale, frequency, background density and background pressure, respectively. With the incompressible flow approximation, the momentum equation can be written as[22]

$$\frac{\partial\boldsymbol{\zeta}}{\partial t}-\varepsilon\nabla\times(\boldsymbol{u}\times\boldsymbol{\zeta})=\frac{\varepsilon}{R}\nabla^2\boldsymbol{\zeta}, \tag{2}$$

where $\boldsymbol{\zeta} = \nabla\times\boldsymbol{u}$ is the dimensionless vorticity. In addition we have the dimensionless system constants

$$\begin{aligned} &R=\frac{U_0a}{\nu}, \quad M^2=\frac{\mathrm{i}\omega a^2}{\nu} \quad \text{and} \\ &\frac{R}{|M|^2}=\varepsilon=\frac{U_0}{\omega a}\ll 1, \end{aligned} \tag{3}$$

where R is the Reynolds number, and M^2 is the frequency parameter. For the characterization of streaming flows, we also define the streaming Reynolds number, R_s, which is interconnected with the above dimensionless constants as follows:

$$R_s=\frac{U_0^2}{\nu\omega}=\varepsilon R=\varepsilon^2|M|^2. \tag{4}$$

For the high-frequency cases that we consider for most ultrasound applications, we take ε as a small parameter that allows the possibility of various types of perturbation expansions. For axially symmetric incompressible flows, the solution can be written in terms of the stream function ψ. In spherical coordinates (r, θ, ϕ), we have

$$\boldsymbol{u}=\nabla\times\left(\frac{\psi}{r\sin\theta}\hat{\boldsymbol{e}}_\phi\right), \tag{5}$$

where $\hat{\boldsymbol{e}}_\phi$ is a unit vector in the azimuthal direction. This formulation satisfies the incompressible continuity equation, $\nabla\cdot\boldsymbol{u} = 0$. The momentum eqn (2) takes the following scalar form in spherical coordinates:

$$\begin{aligned} \frac{\partial}{\partial t}(D^2\psi)+\varepsilon\left[\frac{1}{r^2}\frac{\partial(\psi,D^2\psi)}{\partial(r,\bar{\mu})}+\frac{2}{r^2}D^2\psi\ L\psi\right] \\ =\frac{1}{|M|^2}D^4\psi, \end{aligned} \tag{6}$$

where D^2 is the Stokes operator,

$$D^2=\frac{\partial^2}{\partial r^2}+\frac{(1-\bar{\mu}^2)}{r^2}\frac{\partial^2}{\partial\bar{\mu}^2}, \tag{7}$$

$$L=\frac{\bar{\mu}}{(1-\bar{\mu}^2)}\frac{\partial}{\partial r}+\frac{1}{r}\frac{\partial}{\partial\bar{\mu}}, \tag{8}$$

$\bar{\mu} = \cos\theta$, and the first term multiplying ε is the Jacobian operator,

$$\frac{\partial(P,Q)}{\partial(x,y)}=\frac{\partial P}{\partial x}\frac{\partial Q}{\partial y}-\frac{\partial Q}{\partial x}\frac{\partial P}{\partial y}. \tag{9}$$

This formulation will be applied to various problems, starting with the case of a sphere at the velocity antinode. We refer to this development as Riley's solution.

2 Solid sphere at the velocity antinode: Riley's solution

We discuss Riley's[21] solution since it forms a basis for various analytical results for this class of problems. While Riley[21] considered both $|M| \ll 1$ and $|M| \gg 1$, the latter case (high frequency) is the one relevant to ultrasound levitation.

For a standing wave with velocity (in dimensional variables),

$$u_z'=U_0\cos(kz')e^{\mathrm{i}\omega t'}, \tag{10}$$

the local velocity in the neighbourhood of the antinode ($z' = 0$) is

$$u_z'=U_0\left(1-\frac{1}{2}k^2z'^2+\cdots\right)e^{\mathrm{i}\omega t'}. \tag{11}$$

Here k is the wavenumber given by $k = 2\pi/\lambda$ and $\mathrm{i}=\sqrt{-1}$. With a small particle at the antinode, the surrounding field may just be taken as the first term $u_z' = U_0e^{\mathrm{i}\omega t'}$, whereby Riley's[21] solution is applicable. We scale the dimensional variables according to eqn (1) as well as (3). Writing eqn (5) in component form, we have

$$\begin{aligned} &u_r=-\frac{1}{r^2}\frac{\partial\psi}{\partial\bar{\mu}} \quad \text{and} \\ &u_\theta=-\frac{(1-\bar{\mu}^2)^{-\frac{1}{2}}}{r}\frac{\partial\psi}{\partial r}. \end{aligned} \tag{12}$$

The boundary conditions are

$$\psi=\frac{\partial\psi}{\partial r}=0 \quad \text{on} \quad r=1, \tag{13}$$

and

$$\psi\sim\frac{1}{2}r^2(1-\bar{\mu}^2)e^{\mathrm{i}t} \quad \text{as} \quad r\to\infty. \tag{14}$$

Here and throughout, we have chosen $M\sqrt{2}/|M| = (1+\mathrm{i})$ and ε is defined in eqn (3). The special case $R_s = \varepsilon R \ll 1$ is considered here and Riley's[21] development is summarized next.

2.1 Solution

For $|M| \gg 1$, the vorticity generated at the surface of the sphere is confined to a thin shear-wave layer of dimensional thickness $O(a|M|^{-1})$. We start out with a perturbation expansion,

$$\psi = \psi_0 + \varepsilon\psi_1 + \varepsilon^2\psi_2 + \ldots, \tag{15}$$

and substitute it into the momentum eqn (6). For the leading order, we have for

ψ_0,

$$|M|^2 \frac{\partial(D^2\psi_0)}{\partial t} = D^4\psi_0. \quad (16)$$

The solution for this is expressed by the irrotational field

$$\psi_0 \sim \frac{1}{2}\left(r^2 - \frac{1}{r}\right)(1-\bar{\mu}^2)e^{it}, \quad (17)$$

where it should be noted that both sides of (16) vanish independently since $D^2\psi_0 = 0$. This does not satisfy the no-slip condition, and its validity therefore remains outside the Stokes layer. Within the Stokes layer, an inner layer expansion of the type

$$\Psi = \Psi_0 + \varepsilon\Psi_1 + O(\varepsilon^2) \quad (18)$$

is applied, together with

$$\eta = \frac{1}{2}(r-1)|M|\sqrt{2} = \frac{(r-1)(2R_s)^{1/2}}{2\varepsilon} \quad (19)$$

and

$$\Psi = \frac{1}{2}|M|\psi\sqrt{2} = \frac{(2R_s)^{\frac{1}{2}}\psi}{2\varepsilon}. \quad (20)$$

The variable η represents the radial coordinate stretched in the Stokes-layer region. The leading-order solution is

$$\Psi_0 \sim \frac{3}{2}\left\{\eta - \frac{1}{2}(1-i)\left[1-e^{-(1+i)\eta}\right]\right\} \times (1-\bar{\mu}^2)e^{it}. \quad (21)$$

The order ε term may be decomposed into steady and unsteady components in the form

$$\Psi_1 = \frac{9}{2}\left[\zeta_{20}(\eta) + \zeta_{22}(\eta)e^{2it}\right]\bar{\mu}(1-\bar{\mu}^2), \quad (22)$$

where ζ_{20} and ζ_{22} have been found to be

$$\zeta_{20} = \frac{1}{16}e^{-2\eta} + \frac{5}{4}e^{-\eta}\cos\eta + \frac{3}{4}e^{-\eta}\sin\eta - \frac{1}{2}\eta e^{-\eta}\sin\eta - \frac{21}{16} + \frac{5}{8}\eta, \quad (23)$$

$$\zeta_{22} = \frac{9}{32}(2^{\frac{1}{2}}-1)(1+i) - \left(\frac{9}{32}\right)2^{\frac{1}{2}}(1+i)e^{-(1+i)\eta\sqrt{2}} + \frac{1}{4}(1+i)e^{-(1+i)\eta} + \frac{1}{32}(1+i)e^{-2(1+i)\eta} - \frac{1}{2}ie^{-(1+i)\eta}. \quad (24)$$

At the edge of the Stokes-layer region ($\eta \to \infty$),

$$\Psi \sim \frac{3}{2}\left[\eta\cos t - \left(\frac{1}{2}\right)\sqrt{2}\cos\left(t - \frac{1}{4}\pi\right)\right](1-\bar{\mu}^2) + \frac{9}{32}\varepsilon\left[(-21+10\eta) + \frac{9}{2}\left(2-\sqrt{2}\right) \times \cos\left(2t + \frac{1}{4}\pi\right)\right]\bar{\mu}(1-\bar{\mu}^2) + O(\varepsilon^2). \quad (25)$$

For the outer region where $(r - 1) = O(1)$, using the stream function expansion (15) to $O(\varepsilon)$, the expression for ψ_1 is found to be[21]

$$\psi_1 = -\left(\frac{3}{2R_s^{\frac{1}{2}}r}\right)(1-\bar{\mu}^2) \times \cos\left(t - \frac{1}{4}\pi\right) + \psi_1^{(s)}, \quad (26)$$

where

$$\psi_1^{(s)} = \frac{45}{32}\left(-\frac{1}{r^2} + 1\right)\bar{\mu}(1-\bar{\mu}^2) \quad (27)$$

represents the steady part of the flow field.

2.2 Discussion

The steady outer solution given by eqn (27) exhibits a typical steady streaming flow field as shown in Fig. 3. The important aspect of this flow is that it is a *steady* component arising from its nonlinear character. In view of the thinness of the Stokes layer, including the recirculating region, the outer region streaming behaves as if there was a slip velocity at the surface of the sphere. It is useful to quantify this slip velocity since it can be effectively used to calculate the outer streaming flow field with the application of such a velocity. Using the second part of eqn (12) and applying it to the steady stream function (27), the slip velocity may be expressed as

$$u_\theta^{(slip)} = -\varepsilon\frac{(1-\bar{\mu}^2)^{-\frac{1}{2}}}{r}\frac{\partial\psi_1^{(s)}}{\partial r}\bigg|_{r=1} = -\varepsilon\frac{45}{16}\bar{\mu}(1-\bar{\mu}^2)^{1/2}. \quad (28)$$

This development has been extended to the case of a fluid sphere by Zhao *et al.*,[28] and some interesting observations have been made. This is discussed in detail in tutorial 16.[24] In the next section, we deal with a particle placed at the velocity node of the standing wave.

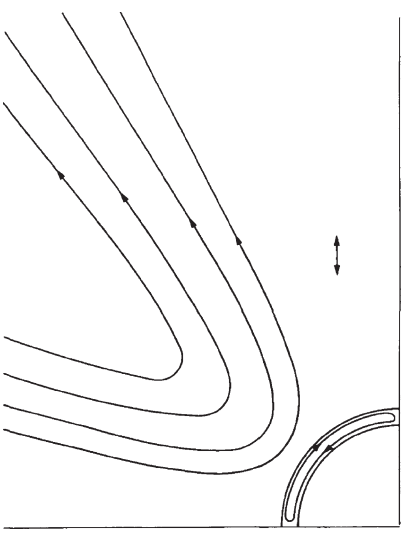

Fig. 3 The streaming flow pattern associated with the steady flow in the case of $|M|^2 \gg 1$, and $R_s \ll 1$. The closed loop is a feature of the Stokes layer. Reproduced from ref. 21.

3 Solid sphere at the velocity node

In the discussion here, the problem of interest concerns the analysis of a solid sphere being placed at the velocity node of the wave. This subsequently leads to an important result for calculating the streaming when the sphere is placed between the velocity node and the anti-node of the wave. We choose axially symmetric spherical polar coordinates (r, θ) fixed in the body of the sphere such that the radial distance r is measured from the center of the sphere and $\theta = 0$ coincides with the axis of oscillation. In this case the equation governing the steady flow in the outer region is Stokes' equation.

3.1 Equations of motion

For the standing wave described in eqn (10), if the origin is shifted to the node, the undisturbed flow (in dimensional form) is

$$u_z' = -U_0\sin(kz')e^{i\omega t'}, \quad (29)$$

and the velocity near the node ($z' = 0$) is

$$u_z' = -U_0\left(kz' - \frac{1}{6}k^3z'^3 + \cdots\right)e^{i\omega t'}. \quad (30)$$

For a small sphere at the node, the first term in the expansion should suffice.

Thus the velocity description for the 'far field' is $u_z' = -U_0 k z' e^{i\omega t'}$.

At the surface of the sphere ($r' = a$), the no-slip boundary conditions given by eqn (13) have to be satisfied. In terms of a velocity potential, the far-field conditions take the form, again in dimensional variables,

$$\varphi'_\infty = \frac{U_0}{k}\left[1 - \frac{1}{2}k^2 r'^2(1-\bar{\mu}^2) + \cdots\right] e^{i\omega t'}. \quad (31)$$

We consider here the Navier–Stokes equation in its compressible form given by eqn (3) in tutorial 13.[23] With the scaling, and the dimensionless parameters being the same as in eqn (1) and (3), the flow description is:

Continuity:

$$\bar{k}^2 \frac{\partial \rho}{\partial t} + \nabla\cdot\boldsymbol{u} + \varepsilon\bar{k}^2 \nabla\cdot\rho\boldsymbol{u} = 0, \quad (32)$$

Momentum:

$$\left[1+\rho\varepsilon\bar{k}^2\right]\frac{\partial \boldsymbol{u}}{\partial t} + \varepsilon\left[1+\rho\varepsilon\bar{k}^2\right]\boldsymbol{u}\cdot\nabla\boldsymbol{u} = -\nabla p + \frac{1}{|M|^2}\nabla^2\boldsymbol{u}, \quad (33)$$

where $\bar{k} = ka$ is the dimensionless wavenumber. The boundary conditions are no-slip on the surface

$$\boldsymbol{u} = \boldsymbol{0} \text{ at } r = 1, \quad (34)$$

and in the far-field,

$$u_z = -\bar{k} z e^{i t}, \quad (35)$$

or equivalently, in the form of a non-dimensional velocity potential,

$$\varphi_\infty = \frac{1}{\bar{k}}\left[1 - \frac{1}{3}\bar{k}^2 r^2 P_2(\bar{\mu}) - \frac{1}{6}\bar{k}^2 r^2\right] e^{i t}, \quad (36)$$

where $P_2(\bar{\mu})$ represents the Legendre polynomial,

$$P_2(\bar{\mu}) = \frac{1}{2}\left(3\bar{\mu}^2 - 1\right). \quad (37)$$

3.2 Solution

Once again, we apply the perturbation procedure,

$$\boldsymbol{u} = \boldsymbol{u}_0 + \varepsilon\boldsymbol{u}_1 + O(\varepsilon^2) \quad (38)$$

$$p = \bar{p}_0 + \varepsilon p_1 + O(\varepsilon^2) \quad (39)$$

$$\rho = \bar{\rho}_0 + \varepsilon\rho_1 + O(\varepsilon^2) \quad (40)$$

on eqn (32) and (33), and construct solutions to $O(1)$ and $O(\varepsilon)$. Here the overbars on $\bar{p}_0$ and $\bar{\rho}_0$ are used to avoid confusion with the background pressure and density.

3.2.1 The leading-order solution. Using the above perturbation expansion in the momentum eqn (33), we obtain

$$\frac{\partial \boldsymbol{u}_0}{\partial t} = -\nabla\bar{p}_0, \quad (41)$$

which, according to our development in tutorial 13,[23] corresponds to irrotational flow, and may be expressed as a velocity potential

$$\boldsymbol{u}_0 = \nabla\varphi_0, \quad (42)$$

and it is not difficult to see that

$$\bar{p}_0 = -\frac{\partial \varphi_0}{\partial t}. \quad (43)$$

This is applicable to the far-field so that with the use of (36),

$$p_\infty = \rho_\infty = -\frac{\partial \varphi_\infty}{\partial t} = -\frac{i}{\bar{k}}\left[1 - \frac{1}{3}\bar{k}^2 r^2 P_2(\bar{\mu}) - \frac{1}{6}\bar{k}^2 r^2\right] e^{i t}. \quad (44)$$

From the continuity eqn (32), the leading-order solution $\boldsymbol{u}_0$ satisfies

$$\bar{k}^2 \frac{\partial \bar{\rho}_0}{\partial t} + \nabla\cdot\boldsymbol{u}_0 = 0. \quad (45)$$

Maintaining order in $\bar{k}$, it is not difficult to see that only the term $(-i/\bar{k})e^{it}$ in $\bar{p}_0$ is needed here. Therefore,

$$\bar{k} e^{i t} + \nabla\cdot\boldsymbol{u}_0 = 0 \quad (46)$$

which may be written in the form of a potential function,

$$\nabla^2\phi_0 + \bar{k} = 0, \quad (47)$$

where φ_0 and ϕ_0 are related by

$$\varphi_0 = \phi_0(r, \theta)\, e^{i t}. \quad (48)$$

Now, applying zero normal velocity on the surface of the sphere, *i.e.*,

$$u_{r0} = \frac{\partial \varphi_0}{\partial r} = 0 \quad \text{at} \quad r = 1, \quad (49)$$

together with the far-field condition (36), we obtain

$$\varphi_0 = \left\{\frac{1}{\bar{k}} - \frac{1}{3}\bar{k}\left(\frac{1}{2}r^2 + \frac{1}{r}\right) - \frac{1}{3}\bar{k}\left(r^2 + \frac{2}{3r^3}\right)P_2(\bar{\mu})\right\} e^{i t}, \quad (50)$$

and

$$\bar{p}_0 = \bar{\rho}_0 = -i\left\{\frac{1}{\bar{k}} - \frac{1}{3}\bar{k}\left(\frac{1}{2}r^2 + \frac{1}{r}\right) - \frac{1}{3}\bar{k}\left(r^2 + \frac{2}{3r^3}\right)P_2(\bar{\mu})\right\} e^{i t}. \quad (51)$$

Being potential flow, the no-slip condition cannot be satisfied, and detailed development in the Stokes layer is needed. In this boundary layer, we write the velocity field in terms of normal (radial) and tangential components,

$$\boldsymbol{u}^b = u_r^b \hat{\boldsymbol{e}}_r + u_\theta^b \hat{\boldsymbol{e}}_\theta. \quad (52)$$

As usual, with $|M|^2 \gg 1$, the vorticity generated at the surface of the sphere is confined to a thin Stokes layer of dimensional thickness $O(a|M|^{-1})$. We scale the inner variables within the Stokes layer as

$$\eta = (r-1)\frac{|M|}{\sqrt{2}}, \quad \text{and} \quad u_\eta^b = \frac{|M|}{\sqrt{2}}u_r^b. \quad (53)$$

Again, perturbing in powers in ε,

$$\boldsymbol{u}^b = \boldsymbol{u}_0^b + \varepsilon\boldsymbol{u}_1^b + O(\varepsilon^2), \quad (54)$$

$$p^b = p_0^b + \varepsilon p_1^b + O(\varepsilon^2), \quad (55)$$

$$\rho^b = \rho_0^b + \varepsilon\rho_1^b + O(\varepsilon^2), \quad (56)$$

and using these expansions (54)–(56) in the momentum eqn (33), we have for the leading-order normal and tangential velocities,

$$\frac{\partial u_{r0}^b}{\partial t} = -\frac{\partial p_0^b}{\partial r} = -\frac{|M|}{\sqrt{2}}\frac{\partial p_0^b}{\partial \eta} \quad (57)$$

and

$$\frac{\partial u_{\theta 0}^b}{\partial t} = -\frac{\partial p_0^b}{\partial \theta} + \frac{1}{2}\frac{\partial^2 u_{\theta 0}^b}{\partial \eta^2}, \quad (58)$$

respectively. The frequency parameter $|M| \gg 1$, and therefore from eqn (57), we may deduce that the leading-order acoustic pressure p_0^b in the boundary layer is a function of θ and t only. Therefore, $\partial p_0^b/\partial\eta = 0$, and using this information in eqn (51), we find

$$p_0^b = \rho_0^b = \bar{p}_0|_{r=1} = -\frac{\mathrm{i}}{\bar{k}}\left[1 - \frac{1}{2}\bar{k}^2 - \frac{5}{9}\bar{k}^2 P_2(\bar{\mu})\right]e^{\mathrm{i}t}. \quad (59)$$

With use of eqn (59) and the boundary condition

$$u_{\theta 0}^b = 0 \text{ as } \eta = 0 \quad (60)$$

in eqn (58), we obtain the differential equation for $u_{\theta 0}^b$ which, when solved, yields

$$u_{\theta 0}^b = \frac{5}{3}\bar{k}\sin\theta\cos\theta\left(1 - e^{-(1+\mathrm{i})\eta}\right)e^{\mathrm{i}t}. \quad (61)$$

Then, from the continuity eqn (32), we obtain the equation for the leading-order normal velocity in the boundary layer $u_{\eta 0}^b$ as

$$\bar{k}^2\frac{\partial \rho_0^b}{\partial t} + \frac{\partial u_{\eta 0}^b}{\partial \eta} + \frac{1}{\sin\theta}\frac{\partial}{\partial \theta}\left(u_{\theta 0}^b \sin\theta\right) = 0. \quad (62)$$

Next, the boundary condition

$$u_{\eta 0}^b = 0 \text{ at } \eta = 0 \quad (63)$$

leads to the solution of $u_{\eta 0}^b$ as

$$u_{\eta 0}^b = \left\{-\bar{k}\eta + \frac{10}{3}\bar{k}\left[-\eta + \frac{1}{2}(1-\mathrm{i}) \times \left(1 - e^{-(1+\mathrm{i})\eta}\right)\right]P_2(\bar{\mu})\right\}e^{\mathrm{i}t}. \quad (64)$$

Here, it should be noted that the first term $-\bar{k}\eta e^{\mathrm{i}t}$ represents the compressibility in the boundary layer.

3.2.2 The first-order solution [$O(\varepsilon)$]. As with most problems in this class, the first-order solution is much more complex than the leading order. Our interest, however, lies in understanding the steady streaming outside the sphere, and we consider only the steady-state solutions here. In this section, therefore, all the first order variables are time-independent, and we shall dispense with the superscript (s) for the steady part. Also, noting the fact that first order is indeed $O(\varepsilon)$, the leading-order of the steady part is $O(\varepsilon)$.

It is not difficult to show that the first-order velocity field is incompressible,[29] *i.e.*, $\nabla\cdot\mathbf{u}_1^b = 0$. Making use of eqn (54)–(56) in the momentum eqn (33), equating both sides in the order of ε, and taking the time average, we have

$$\langle \rho_0^b \bar{k}^2 \frac{\partial u_{\eta 0}^b}{\partial t}\rangle + \langle u_{\eta 0}^b \frac{\partial u_{\eta 0}^b}{\partial \eta}\rangle + \langle u_{\theta 0}^b \frac{\partial u_{\eta 0}^b}{\partial \theta}\rangle = -\frac{|M|^2}{2}\frac{\partial p_1^b}{\partial \eta} + \frac{\partial^2 u_{\eta 1}^b}{\partial \eta^2}, \quad (65)$$

and

$$\langle \rho_0^b \bar{k}^2 \frac{\partial u_{\theta 0}^b}{\partial t}\rangle + \langle u_{\eta 0}^b \frac{\partial u_{\theta 0}^b}{\partial \eta}\rangle + \langle u_{\theta 0}^b \frac{\partial u_{\theta 0}^b}{\partial \theta}\rangle = -\frac{\partial p_1^b}{\partial \theta} + \frac{1}{2}\frac{\partial^2 u_{\theta 1}^b}{\partial \eta^2}, \quad (66)$$

for the first-order normal and tangential velocities, respectively, in the boundary layer. Recognizing once again that $|M|^2 \gg 1$, whereby in eqn (65) the pressure derivative term is dominant, we end up with

$$\frac{\partial p_1^b}{\partial \eta} = 0, \quad (67)$$

which means the first order time-independent pressure in the boundary layer is a function of θ only. Since the steady flow in the boundary layer is incompressible, the velocity field can be written in terms of the stream function ψ_1^b so that

$$u_{r1}^b = \frac{1}{r^2\sin\theta}\left(\frac{\partial \psi_1^b}{\partial \theta}\right), \quad (68)$$

and

$$u_{\theta 1}^b = -\frac{1}{r\sin\theta}\left(\frac{\partial \psi_1^b}{\partial r}\right). \quad (69)$$

Using this stream-function form (eqn (69)) in eqn (66), with the limit $\psi_1^b = o(\eta^2)$ as $\eta\to\infty$, together with the boundary conditions,

$$\psi_1^b = 0 \quad \text{and} \quad \frac{\partial \psi_1^b}{\partial \eta} = 0 \text{ at } \eta = 0,$$

we obtain the solution for ψ_1^b as

$$\psi_1^b = -\frac{\sqrt{2}}{|M|}\bar{k}^2\left\{\left(\frac{25}{72}e^{-2\eta} + \frac{10}{3}e^{-\eta}\cos\eta + \frac{35}{18}e^{-\eta}\sin\eta + \frac{5}{9}\eta e^{-\eta}\sin\eta + \frac{25}{12}\eta - \frac{265}{72}\right)\bar{\mu}(1-\bar{\mu}^2) + \left(-\frac{25}{36}e^{-2\eta} - \frac{100}{9}e^{-\eta}\cos\eta - \frac{125}{18}e^{-\eta}\sin\eta - \frac{25}{6}\eta e^{-\eta}\sin\eta - \frac{50}{9}\eta + \frac{425}{36}\right)\bar{\mu}^3(1-\bar{\mu}^2)\right\}. \quad (70)$$

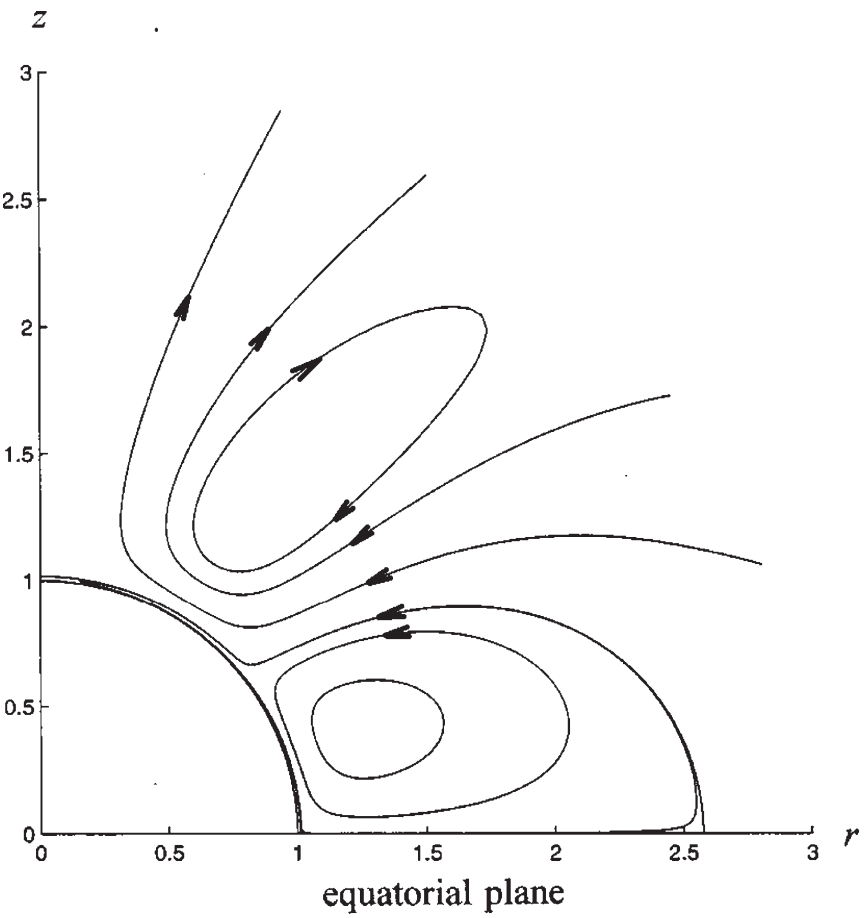

Fig. 4 Streaming in the outer region for a sphere placed at the velocity node. The detail in the Stokes layer is shown in Fig. 4. Reproduced from ref. 29.

The perturbation solution (70) represents an inner solution, corresponding to the Stokes layer. For the outer region where $(r - 1) = O(1)$, we need to construct another asymptotic solution. Again, it is not difficult to demonstrate incompressibility[29] so that $\nabla\cdot\boldsymbol{u}_1 = 0$. Therefore, once more, we introduce the stream function ψ_1, for the outer region this time, such that

$$u_{r1} = \frac{1}{r^2 \sin\theta}\left(\frac{\partial\psi_1}{\partial\theta}\right) \quad \text{and} \quad u_{\theta 1} = -\frac{1}{r\sin\theta}\left(\frac{\partial\psi_1}{\partial r}\right). \tag{71}$$

Equating coefficients of powers of ε in the momentum eqn (33), and using the above stream function relationship, we obtain the Stokes flow equation

$$D^4\psi_1 = 0, \tag{72}$$

where D^2 is the standard Stokes operator given by eqn (7). After asymptotic matching, we obtain the following expression for ψ_1:

$$\psi_1 = \bar{k}^2\left[\frac{25}{168}\left(-r^{-2}+1\right)\bar{\mu}(1-\bar{\mu}^2) + \frac{25}{63}\left(-r^{-4}+r^{-2}\right)(7\bar{\mu}^3-3\bar{\mu})(1-\bar{\mu}^2)\right], \tag{73}$$

again demonstrating the persistence of streaming outside the Stokes layer. As in Section 2.2, we can obtain the slip velocity

$$u_0^{(slip)} = -\varepsilon\frac{(1-\bar{\mu}^2)^{-\frac{1}{2}}}{r}\frac{\partial\psi_1}{\partial r}\bigg|_{r=1} = -\varepsilon\bar{k}^2\left[\frac{25}{84}\bar{\mu}(1-\bar{\mu}^2)^{1/2} + \frac{50}{63}(7\bar{\mu}^3-3\bar{\mu})(1-\bar{\mu}^2)^{1/2}\right]. \tag{74}$$

3.3 Discussion

The streaming flow field in the outer region is depicted in Fig. 4. Here, unlike the sphere at the velocity antinode, the outer region has a pair of toroidal vortices (only one is shown) symmetrical about the equatorial plane. The recirculating part of the Stokes layer does not cover the entire sphere but just the equatorial belt. Over the remaining region in the Stokes layer, the outer flow continues into the Stokes layer. The detail in the Stokes-layer region is not clear in this figure, and is shown on a stretched radial scale in Fig. 5.

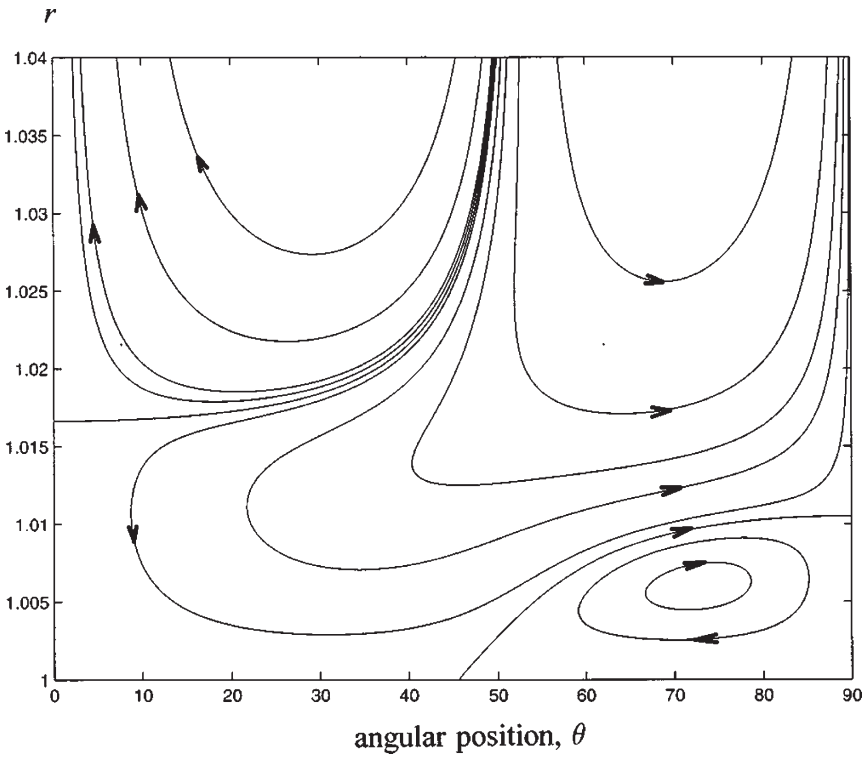

Fig. 5 Detailed flow field in the Stokes layer on the surface with a stretched radial scale. Reproduced from ref. 29.

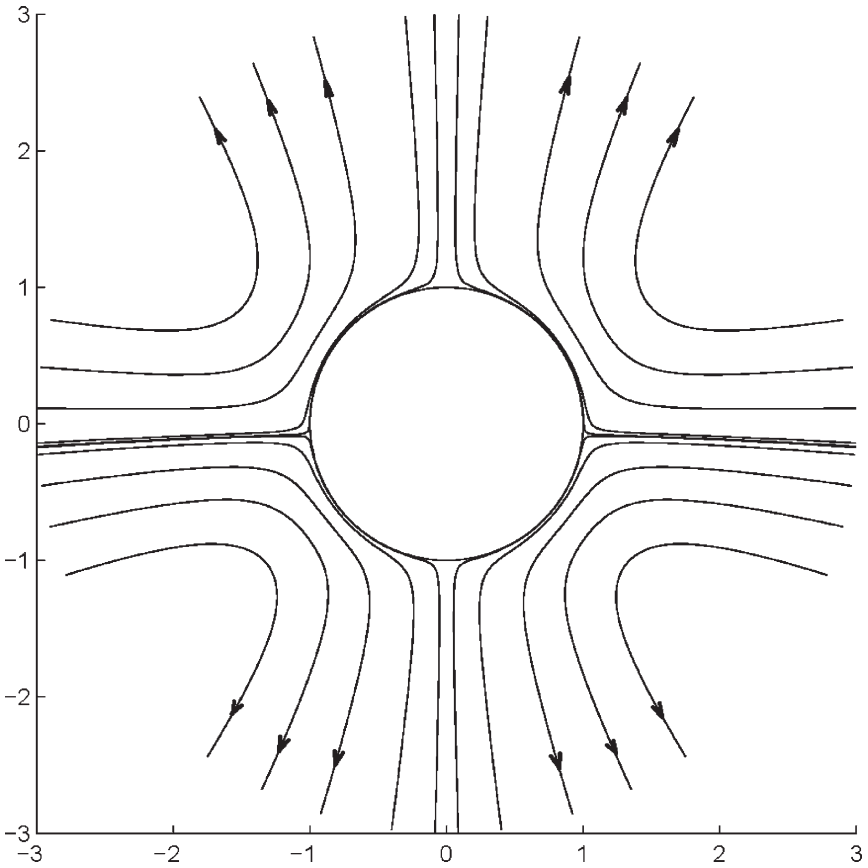

Fig. 6 Streaming about a solid sphere displaced between velocity node and antinode for $\bar{k}z_0 = \pi/8$, $\bar{k} = 0.3$, and $|M| = 800$. With small displacement from the antinode, the flow is nearly symmetric about the equator. Reproduced from ref. 19.

4 Streaming around a sphere placed between nodes

A particle levitated in a gravity field would position itself between the velocity node and the antinode. The analysis of a solid sphere levitated between nodes has been carried out. In this development, use is made of the antinode solution of Riley[21] and the node solution (see previous two sections) through a nonlinear combination. Full calculations within the Stokes layer have been carried out.[19] However, the details of these calculation will not be presented since these can be easily derived from the liquid-drop cases (discussed in tutorial 16[24]) when the infinite-viscosity limit is taken. The basis of the analysis is the expansion of the standing wave for which we express the dimensional velocity u_z' such that[19]

$$u_z' = U_0\cos(kz')e^{i\omega t'} = U_0\cos(\bar{k}z)e^{it} = U_0\,[\cos(\bar{k}z_0) - \bar{k}(z - z_0)\sin(\bar{k}z_0) + O(\bar{k}^2(z - z_0)^2)e^{it}, \quad (75)$$

where we use the previous definition of the dimensionless wavenumber $\bar{k} = ka$. This right-hand side represents the local velocity in the neighbourhood of the sphere centered at $z = z_0$, the dimensionless displacement of the center of the sphere from the velocity antinode. The expansion splits the far-field velocity into solutions about the velocity node and the antinode. While the leading-order irrotational parts combine linearly, the streaming part is nonlinear and there are terms in addition to the node and the antinode solution. This procedure is detailed in tutorial 16[24] for the liquid drop. However, the solid-sphere results are relevant here, and some of them are presented.

We have found that the results are consistent with the outer solution of Lee & Wang.[9] In Fig. 6–8, we can see the streamlines for a solid sphere with $\bar{k}$ = 0.3. It is apparent that the asymmetry about the equator in the streaming pattern when the sphere is away from the velocity antinode is because of the asymmetric distribution of the undisturbed flow. There is stronger streaming on the velocity antinode side where the fluid velocity tends to be higher. Away from the surface of the sphere, the flow pattern does not depend on $|M|$ of course, but on the displacement $\bar{k}z_0$. It is noted that there is a transition value

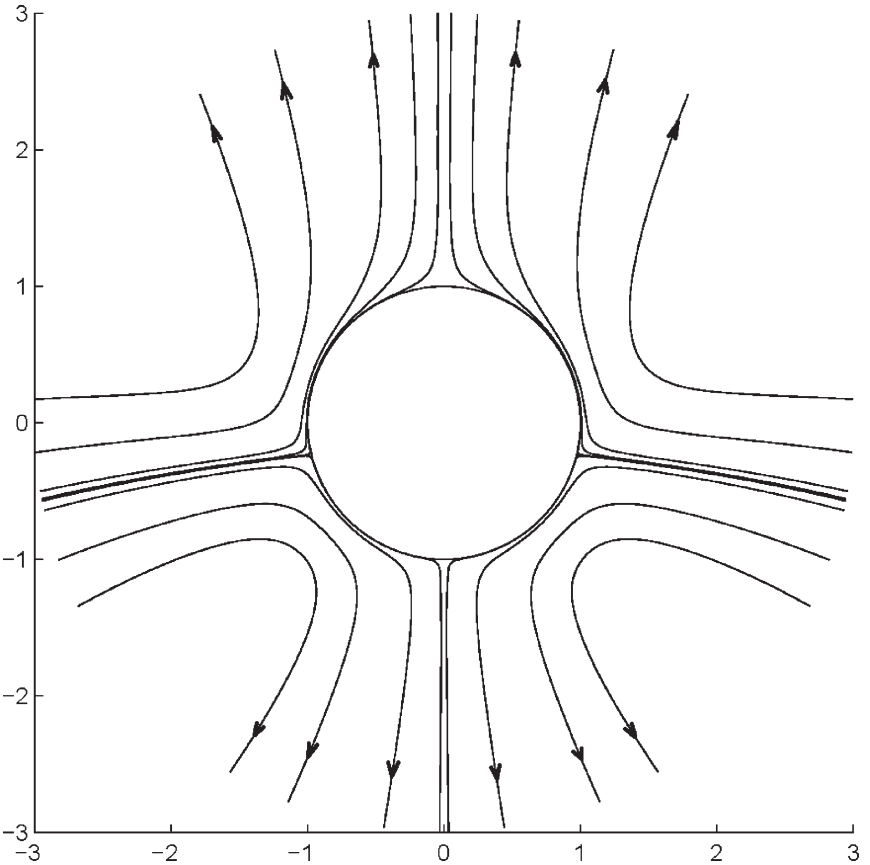

Fig. 7 Streaming about a solid sphere displaced between velocity node and antinode for $\bar{k}z_0 = 5\pi/16$, $\bar{k}$ = 0.3, and $|M|$ = 800. With increasing $\bar{k}z_0$, the equatorial symmetry is broken. Reproduced from ref. 19.

$\bar{k}z_0 = K_0$ (with $5\pi/16 < K_0 < 3\pi/8$) in the flow pattern. When $\bar{k}z_0 < K_0$, there exists a thin recirculating region, limited to the Stokes layer adjacent to the surface, quite similar to that for a solid particle at the velocity antinode. Since this region is quite thin, it is not clearly visible in Fig. 6–7. However, when $\bar{k}z_0 > K_0$, larger vortices appear around the north-pole region, as shown in Fig. 8.

5 Oblate spheroid at the velocity antinode

For non-spherical particles, the analysis increases in complexity, and the set of available analytical results is quite limited. One analytical invesitgation by Rednikov & Sadhal[17] provides a detailed set of results with changes in the aspect ratio for an oblate spheroid. The full analysis is quite elaborate for the scope of this tutorial, and only a limited aspect up to the point of steady streaming in the Stokes layer is being presented. The formal setup of the problem is an oblate spheroid vibrating parallel to the polar axis, much like Riley's[21] problem for a sphere.

5.1 Formulation and results

The scaling of the variables and system constants given by eqn (1) and (3) apply once again. To accommodate the spheroidal geometry, an appropriate spheroidal coordinate system was used. The relationship between cylindrical (ϱ', z', φ) and the oblate spheroidal system $(\lambda, \bar{\mu}, \varphi)$ is

$$z' = c\lambda\bar{\mu}, \quad \varrho' = c\,(1+\lambda^2)^{1/2}(1-\bar{\mu}^2)^{1/2}, \quad (76)$$

with $0 \leqslant \lambda < \infty$, $-1 \leqslant \bar{\mu} \leqslant 1$, $0 \leqslant \phi < 2\pi$.

The parameter c is the focal radius, and the equatorial and polar radii are

$$a = c(1 + \lambda_0^2)^{1/2},\ b = c\lambda_0 \quad (77)$$

respectively, with $\lambda = \lambda_0$ defining the surface of the spheroid (see Fig. 9). With the flow being axially symmetric, eqn (5) can be used (thus satisfying the continuity equation) whereby the velocity components may be expressed nondimensionally

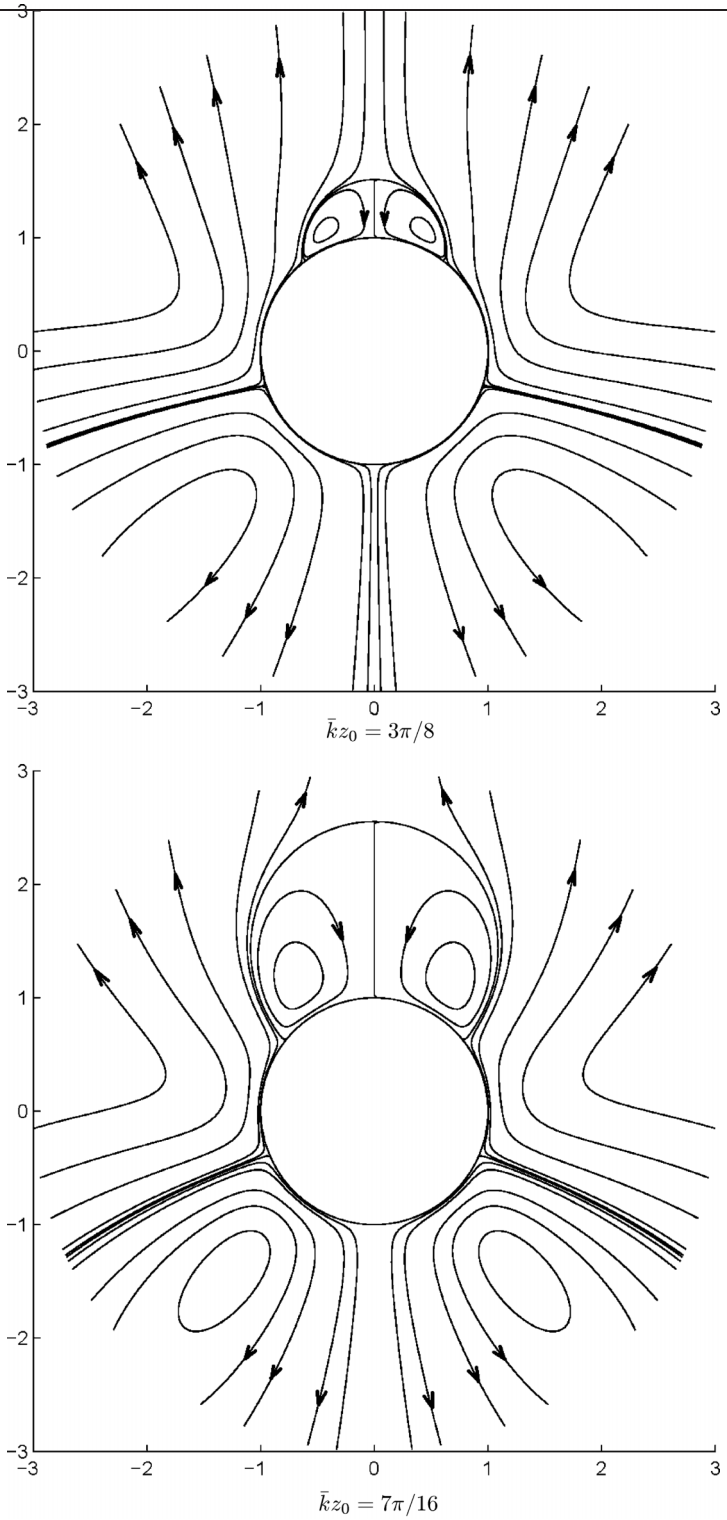

Fig. 8 Streaming about a solid sphere displaced between velocity node and antinode for $\bar{k} = 0.3$, and $|M| = 800$. Close to the node ($\bar{k}z_0 = \pi/2$), vortices develop on the north-pole side. Reproduced from ref. 19.

as[5]

$$u_{\bar{\mu}} = \frac{a^2}{c^2(1-\bar{\mu}^2)^{1/2}(\lambda^2+\bar{\mu}^2)^{1/2}}\frac{\partial\psi}{\partial\lambda}, \qquad u_{\lambda} = -\frac{a^2}{c^2(1+\lambda^2)^{1/2}(\lambda^2+\bar{\mu}^2)^{1/2}}\frac{\partial\psi}{\partial\bar{\mu}}. \tag{78}$$

For the purpose of nondimensionalization, we are using the major radius a as a length scale. For this case of incompressible axisymmetric flow, eqn (6) for the conservation of momentum is applicable. We shall not give the details which are available in ref. 17.

The boundary conditions consist of oscillatory flow parallel to the polar axis at infinity, and the usual no-slip and non-penetration at the solid surface of the spheroidal particle. Thus, in the far-field, $\psi = \frac{1}{2}(\varrho/a)^2 e^{it}$, and with the transformation (76) we obtain

$$\lambda\to\infty : \psi \to \frac{1}{2}(c/a)^2(1+\lambda^2)(1-\bar{\mu}^2)e^{it}. \tag{79}$$

At the surface of the oblate spheroid, we have

$$\lambda = \lambda_0 : \quad \psi = \frac{\partial\psi}{\partial\lambda} = 0. \tag{80}$$

As for most streaming flow analyses involving solid boundaries, the problem here is singular and requires the detail in the Stokes layer. Within this layer, we use the inner variables which entail stretching of the coordinate in the direction normal to the solid surface. With the dimensional layer thickness being $O(a/|M|)$, we write

$$Y = \frac{(c/a)(\lambda_0^2+\bar{\mu}^2)^{1/2}}{(1+\lambda_0^2)^{1/2}}|M|(\lambda-\lambda_0) \tag{81}$$

and

$$\Psi = |M|\psi. \tag{82}$$

Leading order oscillatory flow. Sparing all the detail, the solution for the outer irrotational flow is found to be[17]

$$\psi^{(u)} = \frac{(c/a)^2}{2}\left[1+\lambda^2-(1+\lambda_0^2)\times\frac{(1+\lambda^2)\ \mathrm{arccot}(\lambda)-\lambda}{(1+\lambda_0^2)\ \mathrm{arccot}(\lambda_0)-\lambda_0}\right](1-\bar{\mu}^2)e^{it}, \tag{83}$$

and for the Stokes layer,

$$\Psi^{(u)} = \frac{A(1+\lambda_0^2)^{1/2}}{(\lambda_0^2+\bar{\mu}^2)^{1/2}}\times\left\{Y-\frac{1}{\sqrt{\mathrm{i}}}\left[1-e^{-\sqrt{\mathrm{i}}Y}\right]\right\}(1-\bar{\mu}^2)e^{it} \tag{84}$$

where $\sqrt{\mathrm{i}} = (1+\mathrm{i})/\sqrt{2}$ and

$$A = \frac{(c/a)}{(1+\lambda_0^2)\ \mathrm{arccot}(\lambda_0)-\lambda_0}. \tag{85}$$

The superscript (u) refers to the unsteady flow. Next, we consider the steady part of the flow in the Stokes layer.

Steady streaming in the Stokes layer. Again, leaving out all the details, the $O(\varepsilon)$ result in the Stokes layer, keeping only the steady part denoted by the superscript (s), is

$$\Psi^{(s)} = A^2 \frac{(1+\lambda_0^2)^{1/2}\,\bar{\mu}(1-\bar{\mu}^2)}{\sqrt{2}(c/a)^2(\lambda_0^2+\bar{\mu}^2)^{3/2}} \times \left[f_1\left(\frac{Y}{\sqrt{2}}\right)\frac{1-\bar{\mu}^2}{\lambda_0^2+\bar{\mu}^2} + f_2\left(\frac{Y}{\sqrt{2}}\right)\right] \quad (86)$$

with

$$f_1(z) = ze^{-z}\sin z + 3e^{-z}\cos z + 2e^{-z}\sin z + \frac{1}{4}e^{-2z} + \frac{3}{2}z - \frac{13}{4}, \quad (87)$$

$$f_2(z) = 2ze^{-z}\sin z + 5e^{-z}\cos z + 3e^{-z}\sin z + \frac{1}{4}e^{-2z} + \frac{5}{2}z - \frac{21}{4}, \quad (88)$$

and A is given by eqn (85). It should be noted here that the ordering for the steady and unsteady flows corresponds to $\Psi = \Psi^{(u)} + \varepsilon\Psi^{(s)}$. We now examine the edge of the Stokes layer by letting $Y \to \infty$. Upon examining $\partial\Psi^{(s)}/\partial Y$ as $Y \to \infty$, we see that there is a nonzero velocity in the direction which is tangential to the solid surface. Detailed calculations[17] show that the effective slip velocity is

$$u^{(slip)} \equiv u_{\bar{\mu}}^{(s)}|_{Y\to\infty} = \frac{A^2}{4(c/a)^3}\left[3\frac{\bar{\mu}(1-\bar{\mu}^2)^{3/2}}{(\lambda_0^2+\bar{\mu}^2)^{5/2}} + 5\frac{\bar{\mu}(1-\bar{\mu}^2)^{1/2}}{(\lambda_0^2+\bar{\mu}^2)^{3/2}}\right]. \quad (89)$$

The sign of the slip velocity in eqn (89) is such that the flow takes place from the equator towards the poles. The distribution (89) is shown in Fig. 10 for various aspect ratios of the oblate spheroid.

In place of the coordinate , the scaled distance s along the surface is used with $-1 \leqslant s \leqslant 1$ and $s = 0$ defined to be at the equator of the spheroid, while $s = \pm 1$ correspond to the poles. In view of the symmetry with respect to the equatorial plane, the distribution over only one hemisphere is shown in Fig. 10. For any given aspect ratio b/a, the parameter λ_0 is determined from (77) for a given value of b/a while $c = a/(1 + \lambda_0^2)^{1/2}$.

5.2 Discussion

The streamlines for the steady flow in the Stokes layer are represented in Fig. 11 corresponding to eqn (86). Here the vertical scale is highly exaggerated, and again the scaled relative distance along the surface is used in the plot.

The results depicted in Fig. 10 and 11 show that the streaming intensity sharply increases with decreasing the ratio b/a of the oblate spheroid, the other constraints being the same. Besides, as the intensity increases, the center of the streaming (location of the maximum intensity) becomes strongly displaced towards the sharp edge (equatorial plane, $s = 0$) of the particle. Another effect of the aspect ratio change is that the streamlines become much denser around the sharp-edged equator than they are in other parts of the region when b/a gets smaller. The zone of recirculation covers the entire spheroid in a manner quite similar to that of a sphere (Fig. 11). However, in contrast from the sphere, the thickness of this zone becomes slightly nonuniform.

Among the major purposes of this study was to see how changes in the aspect ratio and the deviation from sphericity play into the streaming behavior of the flow field. It is therefore of interest to discuss the asymptotic behavior of the streaming characteristics as the ratio of the minor to the major axes, b/a, tends to zero as for the circular disk limit (*i.e.*, $\lambda_0 \to 0$). For this illustration, λ_0 is chosen as the smallness parameter, and the scalings for the variables $u_{\bar{\mu}}^{(s)}$, s and $\bar{\mu}$ are established in the zone of the most intense streaming. These are obtained by following the maximum of the effective slip velocity (89). From eqn (77), the geometric parameters can be examined for small λ_0. Simple expansions yield

$$b/a = \lambda_0 + O(\lambda_0^3), \quad a/c = 1 + O(\lambda_0^2), \text{ as } \lambda_0 \to 0. \quad (90)$$

From (89), and following the detailed calculations of Rednikov & Sadhal,[17] we obtain

$$u_{\bar{\mu}}^{(s)} = O(\lambda_0^{-4}), \quad s = O(\lambda_0^2),\ \bar{\mu} = O(\lambda_0) \text{ as } \lambda_0 \to 0 \quad (91)$$

from which we can see that $u_{\bar{\mu}}^{(s)} \sim 1/s^2$, a characteristic observed in Fig. 10 for small λ_0.

It is also noteworthy that the radius of curvature R_c taken at the sharp-edged equator of the oblate spheroid is

$$R_c/a = O(\lambda_0^2) \text{ as } \lambda_0 \to 0. \quad (92)$$

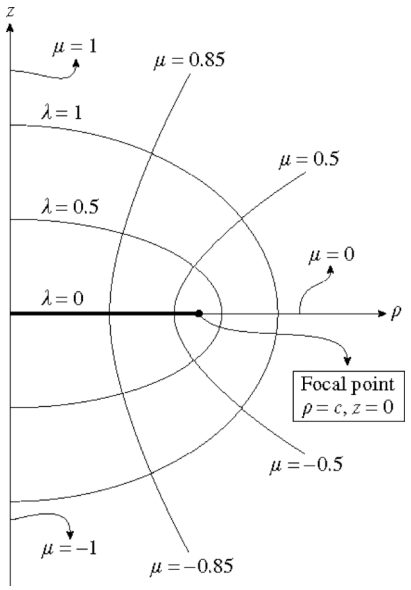

Fig. 9 Schematic of the oblate spheroidal coordinate system. Reproduced from ref. 17.

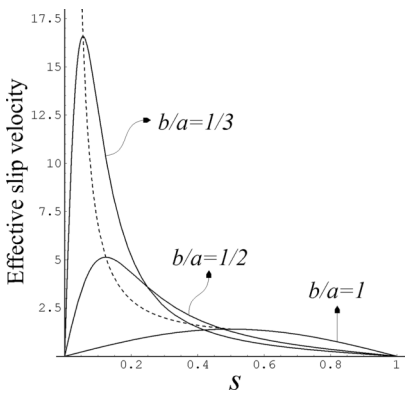

Fig. 10 Slip velocity distribution as a function of scaled distance from the equator for various values of b/a. Reproduced from ref. 17.

Considering that $s \sim R_c/a$ as $\lambda_0 \to 0$, we can interpret that the most intense streaming occurs on the scale of the equatorial radius of curvature which turns out to be a significant parameter for streaming intensity. With detailed scaling arguments,[17] it is shown that to maintain validity of the results close to the disk limit ($\lambda_0 \to 0$), the flow parameters ε and $|M|$ need to be more restrictive than $\varepsilon \ll 1$ and $|M|^2 \gg 1$. The radius of curvature becomes a relevant length scale for this purpose, and for the Stokes layer to remain thin,

$$\tilde{\varepsilon} \sim \frac{\varepsilon}{\lambda_0^3} \ll 1, \qquad |\tilde{M}|^2 \sim |M|^2\lambda_0^4 \gg 1. \quad (93)$$

There has been considerably more work done on this problem,[17] particularly

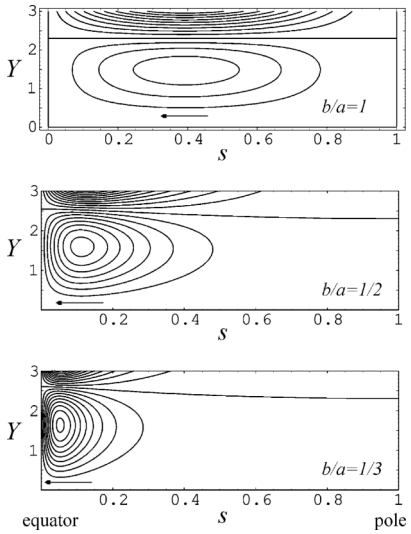

Fig. 11 Streamlines in the Stokes layer for various values of b/a. Here $s = 0$ corresponds to the equator and $s = 1$ to the pole of the spheroid. The vertical scale is stretched coordinate normal to the spheroid. Reproduced from ref. 17.

in relation to streaming outside the Stokes layer. It turns out that for $R_s \ll 1$, to the leading order ($O(\varepsilon)$ in this case), the outer streaming is described by the fourth-order Stokes equation for the stream function, and the use of the non-penetration boundary condition together with the slip velocity (89) gives the flow field. While the outer streaming flow field is quite interesting, and changing the aspect ratio leads to substantial deviation from the sphere case, the discussion is outside the scope of this tutorial which is kept limited to the Stokes layer for this problem.

6 Conclusions

In this tutorial, we have provided techniques for tackling streaming-flow problems that arise when solid particles interact with sound waves. The cases of a sphere at the velocity antinode (pressure node) and the velocity node (pressure antinode) of a standing wave have been presented, and dealt with analytically by the singular perturbation method. With all cases considered, a typical small dimensionless parameter $\varepsilon = (U_0/\omega a) \ll 1$, coupled with the frequency parameter $|M|^2 = \omega a^2/\nu \gg 1$, facilitate the analysis. Considerable depth of understanding is achieved with limiting cases of the streaming Reynolds number $R_s = U_0^2/\omega\nu = \varepsilon^2|M|^2$ being small. This is the Reynolds number associated with the mean time-independent flow that arises as a result of the nonlinear interaction of the sound wave with a solid surface. It has been established that for the flow parameters under consideration, the leading-order streaming flow is typically an order higher than the primary oscillatory flow.

Also presented was the situation corresponding to a spherical particle between nodes, followed by an oblate spheroid at the velocity antinode. The first case of a particle at the velocity antinode is mathematically equivalent to a sphere vibrating in an otherwise quiescent fluid, provided the wavelength is large compared with the particle size. The analysis can be carried out with the incompressible flow approximation. The interesting aspect of the streaming flow field is the existence of a thin recirculating zone at the surface of the sphere. Such a zone is also present in the case of a sphere placed at the velocity node. However, the recirculating region does not envelope the entire sphere but rather just an equatorial belt with coverage depending on the flow parameters. The calculations for this flow field demand the compressible flow analysis which does not lend itself so easily to the usual stream function formulation that works for axisymmetric flow.

The flow field for the case of the sphere between nodes is a nonlinear combination of the node and antinode solutions. The results are more interesting with the presence of vortices corresponding to the streaming in the Stokes layer as well as the bulk region. In particular, there are full toroidal vortices present near the polar region of the oncoming streaming flow, qualitatively resembling the visualization exhibited in Fig. 2. However, it is possible to attribute such vortices to the presence of chamber walls of a levitation system.[15]

The analysis of an oblate spheroid at the velocity antinode, while a complex problem, is interesting from the standpoint of changing aspect ratio and edge curvature. The results presented here were limited to the steady streaming in the Stokes layer. With increasing major to minor axis ratio, the streaming vortices in the Stokes layer shift towards the equator. Also seen is an increase in the streaming intensity with this aspect ratio increase. The radius of curvature about the equator is an important determinant for this streaming intensity which varies inversely with the radius. Not surprisingly therefore, the slip velocity near the equatorial region is in inverse proportion to the square of the radius of curvature.

In this tutorial we have presented a limited set of results concerned with acoustic streaming that takes place when ultrasound waves interact with solid particles. In particular, for $\varepsilon \ll 1$ and $|M| \gg 1$, there is intense streaming in the thin Stokes layer near the boundary. The streaming propagates into the bulk of the fluid with intensities an order higher in ε than the leading-order flow. It should be noted that the bulk streaming (*i.e.*, outside the Stokes layer) can be analyzed by considering an effective slip velocity on the boundary.[8,11,18] As far as the streaming phenomenon is concerned, there are several other interesting results such as the effect of two orthogonal ultrasound beams interacting with a particle.[8,16] With the beams being coherent but out of phase by $\pi/2$, there is a net torque on the particle which, if free to move, rotates. This mechanism has been used with levitation work when it is desired to spin a levitated particle.[20] Streaming phenomenon is also seen when a particle experiences rotational oscillations in an otherwise quiescent fluid.[3] However, it is not immediately obvious if an ultrasound wave would produce an equivalent flow field.

Acknowledgements

The author is deeply indebted to Prof. Norman Riley (University of East Anglia) and Dr Alexey Rednikov (Université Libre de Bruxelles), both of whom have imparted their knowledge and experience on the subject of acoustics to him.

References

1 H. Bruus, Acoustofluidics 2: Perturbation theory and ultrasound resonance modes, *Lab Chip*, 2012, **12**, 20–28.
2 M. Evander, L. Johansson, T. Lilliehorn, J. Piskur, M. Lindvall, S. Johansson, M. Almqvist, T. Laurell and J. Nilsson, Noninvasive acoustic cell trapping in a microfluidic perfusion system for online bioassays, *Anal. Chem.*, 2007, **79**, 2984–2991.

3 A. Gopinath and A. F. Mills, Convective heat transfer from a sphere due to acoustic streaming, *J. Heat Transfer*, 1993, **115**, 332–341.
4 S. M. Hagsäter, T. G. Jensen, H. Bruus and J. P. Kutter, Acoustic resonances in microfluidic chips: full-image micro-PIV experiments and numerical simulations, *Lab Chip*, 2007, **7**, 1336–1344.
5 J. Happel and H. H. Brenner, *Low Reynolds Number Hydrodynamics*, Prentice-Hall, 1965.
6 L. V. King, On the acoustic radiation pressure on spheres, *Proceeding of the Royal Society of London*, 1934, **A147**, 212–240.
7 L. V. King, On the acoustic radiation pressure on circular discs: Inertia and diffraction corrections, *Proc. R. Soc. London, Ser. A*, 1935, **153**, 1–16.
8 C. P. Lee and T. G. Wang, Near-boundary streaming around a small sphere due to two orthogonal standing waves, *J. Acoust. Soc. Am.*, 1989, **85**, 1081–1088.
9 C. P. Lee and T. G. Wang, Outer acoustic streaming, *J. Acoust. Soc. Am.*, 1990, **88**, 2367–2375.
10 Y.-H. Lee and C.-A. Peng, Enhanced retroviral gene delivery in ultrasonic standing wave fields, *Gene Ther.*, 2005, **12**, 625–633.
11 W. L. Nyborg, Acoustic streaming near a boundary, *J. Acoust. Soc. Am.*, 1958, **30**, 329–339.
12 K. Ohsaka, A. Rednikov, S. S. Sadhal and E. H. Trinh, Noncontact technique for determining viscosity from shape relaxation of ultrasonically levitated and initially elongated drops, *Rev. Sci. Instrum.*, 2002, **75**, 2091–2095.
13 K. Ohsaka, S. S. Sadhal and A. Rednikov, Thermocapillary flow induced by laser-heating of an acoustically levitated flattened glycerin drop, *J. Heat Transfer*, 2002, **124**, 599.
14 Lord Rayleigh, On the circulation of air observed in Kundt's tubes and some allied acoustical problems, *Philos. Trans. R. Soc. London*, 1884, **175**, 1–21.
15 A. Rednikov and N. Riley, A simulation of streaming flows associated with acoustic levitators, *Phys. Fluids*, 2002, **14**, 1502–1510.
16 A. Rednikov, N. Riley and S. S. Sadhal, The behaviour of a levitated particle in orthogonal acoustic fields, *J. Fluid Mech.*, 2003, **486**, 1–20.
17 A. Rednikov and S. S. Sadhal, Steady streaming from an oblate spheroid due to vibrations along its axis, *J. Fluid Mech.*, 2004, **499**, 345–380.
18 A. Rednikov and S. S. Sadhal, Acoustic/steady streaming from a motionless boundary and related phenomena: generalized treatment of the inner streaming and examples, *J. Fluid Mech.*, 2011, **667**, 426–462.
19 A. Rednikov, H. Zhao, S. S. Sadhal and E. H. Trinh, Steady streaming around a spherical drop displaced from the velocity antinode in an acoustic levitation field, *Q. J. Mech. Appl. Math.*, 2006, **59**, 377–397.
20 W. K. Rhim, S. Chung and D. Elleman, Experiments on rotating charged liquid drops., *In AIP Conf. Proc. 197, Drops and Bubbles, Third International Colloquim, pages*, 1988, 91–105.
21 N. Riley, On a sphere oscillating in a viscous liquid, *Q. J. Mech. Appl. Math.*, 1966, **19**, 461–472.
22 N. Riley, Steady streaming, *Annu. Rev. Fluid Mech.*, 2001, **33**, 43–65.
23 S. S. Sadhal, Acoustofluidics 13: Analysis of acoustic streaming by perturbation methods, *Lab Chip*, 2012, **12**, 2292–2300.
24 S. S. Sadhal, Acoustofluidics 16: Acoustics streaming near liquid-gas interfaces: drops and bubbles, *Lab Chip*, 2012, in press.
25 H. Schlichting, Berechnung ebener periodischer Grenzchichtströmungen, *Physik Zeitschr.*, 1932, **23**, 327–335.
26 E. H. Trinh and J. L. Robey, Experimental studies of streaming flows associated with ultrasonic levitators., *Phys. Fluids*, 1994, **6**, 3567–3579.
27 M. Wiklund, R. Green and M. Ohlin, Acoustofluidics 14: Applications of acoustics streaming in microfluidic devices, *Lab Chip*, 2012, **12**, DOI: 10.1039/c2lc40203c.
28 H. Zhao, S. S. Sadhal and E. H. Trinh, Internal circulation in a drop in an acoustic field, *J. Acoust. Soc. Am.*, 1999, **106**, 3289–3295.
29 H. Zhao, S. S. Sadhal and E. H. Trinh, Singular perturbation analysis of an acoustically levitated sphere: Flow about the velocity node, *J. Acoust. Soc. Am.*, 1999, **106**, 589–595.